MOLECULAR IMAGING AND BIOLOGY

Mol Imaging Biol (2015) 17:512–520
DOI: 10.1007/s11307-014-0815-3

Published Online: 6 January 2015

RESEARCH ARTICLE

Evaluation of the Metabolic Activity of *Echinococcus multilocularis* in Rodents Using Positron Emission Tomography Tracers

Anna-Maria Rolle,[1] Peter T. Soboslay,[2] Gerald Reischl,[1] Wolfgang H. Hoffmann,[2] Bernd J. Pichler,[1] Stefan Wiehr[1]

[1]*Werner Siemens Imaging Center, Department of Preclinical Imaging and Radiopharmacy, Eberhard Karls University, Röntgenweg 13, 72076, Tübingen, Germany*
[2]*Institute for Tropical Medicine, Eberhard Karls University, Tübingen, Germany*

Abstract
Purpose: 2-Deoxy-2-[^{18}F]fluoro-D-glucose ([^{18}F]FDG) has been used as a standard clinical positron emission tomography (PET) tracer for the follow-up of the rare but life-threatening parasitic disease alveolar echinococcosis (AE). Given that the disease is endemic in many countries in the northern hemisphere and the diagnosis is still challenging, the aim of our study was to evaluate further clinically relevant PET tracers as possible diagnostic tools for AE *in vitro* and *in vivo*.
Procedures: Various clinically used PET tracers were evaluated *in vitro* and assessed in an *in vivo* AE animal model based on PET/magnetic resonance (MR) measurements.
Results: In vitro binding assays displayed high uptake of [^{18}F]FDG in a cell suspension of *E. multilocularis* tissue, whereas 3′-deoxy-3′-[^{18}F]fluorothymidine ([^{18}F]FLT) and [^{11}C]choline were found to be taken up strongly by *E. multilocularis* vesicles. [^{18}F]FDG and [^{18}F]FLT displayed an elevated uptake *in vivo*, which appeared as several foci throughout the parasite tissue as opposed to [^{18}F]fluoro-azomycinarabinofuranoside ([^{18}F]FAZA) and [^{11}C]choline.
Conclusions: Our data clearly demonstrate that the clinically applied PET tracer [^{18}F]FDG is useful for the diagnosis and disease staging of AE but also has drawbacks in the assessment of currently inactive or metabolically weak parasitic lesions. The different tested PET tracers do not show the potential for the replacement or supplementation of current diagnostic strategies. Hence, there is still the need for novel diagnostic tools.

Key words: PET/MR, [^{18}F]FDG, [^{18}F]FLT, [^{18}F]FAZA, [^{11}C]choline, *Echinococcus multilocularis*, Alveolar echinococcosis

Introduction

The rare and chronic zoonotic parasitic disease alveolar echinococcosis (AE) is caused by the larval form (metacestode) of the cestode *Echinococcus multilocularis*, known as the fox tapeworm [1, 2]. This cancer-mimicking disease is detected in the northern hemisphere including Middle and Eastern Europe, North America, Northern Asia, China, and Japan [1, 3]. To date, there have been no reports that the disease has spread to the southern hemisphere or the UK [4]. After ingestion of eggs containing an embryonic stage of *E. multilocularis* (oncosphere) shed by the definitive hosts (mainly foxes but also other wild canids), the hatched metacestode invades various organs of the intermediate host

Correspondence to: Stefan Wiehr; *e-mail:* stefan.wiehr@med.uni-tuebingen.de

(rodents, lagomorpha) and aberrant host (humans) causing one of the most lethal helminthic infections in humans [1]. The disease is characterized by an exogenous tumor-like proliferation of the metacestodes predominantly in the liver, which produces symptoms of biliary obstruction, portal hypertension, pain in the upper abdominal region, growing malaise, and weight loss [5]. In the advanced stage of the infection, the parasite disseminates via the blood or lymphatic vessels to other adjacent organs including the lungs but also to the brain [6]. The proliferation of the metacestode is accompanied by invading immune cells around the multi-chambered cystic structures causing inflammation and necrosis in the periparasitic granuloma [7, 8]. Surgical resection of AE, the first treatment choice according to the World Health Organization (WHO) Informal Working Group on Echinococcosis (IWGE) expert consensus [5, 9], is often difficult because of the numerous small vesicles and the diffuse tubular growth pattern in the infected organs [10]. The entire parasite tissue has to be removed to prevent recurrence, which is often not possible due to the long clinical latency and the resultant late stage of infection at diagnosis. Surgical treatment is always accompanied by chemotherapy using the benzimidazole (BZM) carbamate derivatives, mebendazole or albendazole, temporally after complete resection or for life in cases in which surgery is not possible or is incomplete. These drugs are not parasitocidal but act parasitostatic when taken for lifetime, resulting in severe side effects [11]. Therefore, cyclic discontinuation of therapy is indicated, if the parasitic mass does not show signs of metabolic activity in 2-deoxy-2-[^{18}F]fluoro-D-glucose positron emission tomography ([^{18}F]FDG-PET) examinations [12, 13]. However, the confirmation of non-viable *E. multilocularis* tissue after a long treatment duration is crucial.

Imaging techniques such as ultrasonography, computed tomography (CT), magnetic resonance imaging (MRI), and PET are used for the diagnosis and identification of cystic lesions for AE [14]. Immunodiagnostic tools such as enzyme-linked immunosorbent assays (ELISAs) and polymerase chain reaction (PCR) are used to confirm imaging findings [15]. Recently, [^{18}F]FDG-PET with its functional information has been used for follow-up in patients after treatment because the conventional morphological imaging methods depict non-reliable predictive factors for parasite activity [16–18].

Molecular imaging with PET displays the metabolic parameters of living cells and might be able to distinguish between normal and infected tissue based on the use of various PET tracers. One such tracer is [^{18}F]FDG, a fluorinated analog of glucose that is often used in PET and is the clinical gold standard in oncology for primary diagnosis, accurate staging, and detection of metastasis but is also used for diagnosis of infectious diseases [19]. It is transported through the Glut-1 and Glut-3 glucose transporters [20, 21]. The F-18-radiolabelled thymidine derivate 3′-deoxy-3′-[^{18}F]fluorothymidine ([^{18}F]FLT) is a marker of cell proliferation and is consumed by proliferating cells via the salvage pathway that incorporates nucleotides into replicating DNA during the S phase of the cell cycle [22]. [^{11}C]choline, another promising tracer that detects membrane synthesis, is first phosphorylated within the cell and then trapped into lecithin of the cell membrane as phosphatidylcholine [23]. Hypoxic regions can be identified using the ^{18}F-fluoro-azomycinarabinofuranoside ([^{18}F]FAZA), a 2-nitroimidazole PET tracer. [^{18}F]FAZA is diffusible through cell membranes and undergoes reversible reduction. Therefore, with decreasing intracellular concentration of oxygen, the tracer accumulates within the hypoxic tissue [24].

The aim of our study was to evaluate several well-known PET tracers [^{18}F]FLT, [^{18}F]FAZA, and [^{11}C]choline to improve the diagnosis and therapy monitoring of AE. To our knowledge, it was the first study of this kind, where several PET tracers were investigated *in vitro* and *in vivo* for their potential of supporting clinicians in the decision making in regard to therapy disruption in AE patients. In the present study, we used a secondary murine AE model where metacestodes are injected intraperitoneally (i.p.) into Mongolian jirds (*Meriones unguiculatus*) [11, 25]. In this model, the parasite develops tumor-like properties and invades adjacent tissues and organs [26]. With preclinical imaging methods using dedicated small animal PET and MRI, the development and progression of the parasite growth can be monitored *in vivo* without dissecting the animals at different time points, significantly reducing the required animal numbers and obtaining results in a cohort of animals [27]. For the evaluation of the metabolic activity of *E. multilocularis*, we used the abovementioned PET tracers, [^{18}F]FDG, [^{18}F]FLT, [^{18}F]FAZA, and [^{11}C]choline, at two different time points and infection stages (early and late).

In our study, the *in vitro* assays revealed elevated uptake of the tested tracers and showed great potential for *in vivo* application, but only [^{18}F]FDG and [^{18}F]FLT turned out to be suitable for the detection of *E. multilocularis* tissue surrounded by metabolically active inflammatory cells in our animal model. To our knowledge, this is the first time that various clinically established PET tracers have been evaluated in a preclinical setting for the diagnosis of the life-threatening disease, AE.

Materials and Methods

In Vitro Culture of E. multilocularis Metacestodes

Metacestode tissue was aseptically dissected from the peritoneal cavity of experimentally infected gerbils (*M. unguiculatus*) and incubated in cultivation medium (RPMI, 10 % FCS, 1 % penicillin/streptomycin; Biochrom GmbH, Berlin, Germany) at 37 °C and 5 % CO_2. The medium was changed once a week until newly produced metacestode vesicles reached a diameter of 2 to 4 mm.

The *E. multilocularis* vesicles were collected from the cell culture and used for *in vitro* binding assays.

Animal Model of Alveolar Echinococcosis in M. unguiculatus

Ethics Statement

All animal procedures were conducted according to the German Animal Welfare Act, and the animal care and use protocol was approved by the Regierungspräsidium Tübingen.

Ten-week-old female gerbils (*M. unguiculatus*) were purchased from Janvier Labs (Saint-Berthevin Cedex, France). The animals were kept under standardized and sterile environmental conditions (20±1 °C room temperature, 50±10 % relative humidity, 12 h light–dark cycle) and received food and water *ad lib. E. multilocularis* metacestode tissue was maintained routinely in gerbils by serial implantation of parasite tissue as described previously with minor modifications [26]. In brief, metacestode tissue was ground through a metal tea strainer, and 0.5 g of the metacestode cell suspension was intraperitoneally injected into the animals. During the procedure, gerbils were anesthetized with 2 % isoflurane mixed with 100 % oxygen. After sufficient growth of the parasitic mass, the animals were euthanized with CO_2, and the metacestode tissue was removed and used for *in vitro* cell culture or *in vitro* binding assays.

PET Tracer Production

Fluorine-18 was produced as [^{18}F]fluoride at the PETtrace cyclotron (General Electric Medical Systems, GEMS, Uppsala, Sweden) using the $^{18}O(p,n)^{18}F$ nuclear reaction, and [^{18}F]FDG, [^{18}F]FLT, and [^{18}F]FAZA were synthesized as described elsewhere [28–31]. [^{11}C]choline was synthesized from *N*,*N*-dimethylethanolamine (DMAE) by alkylation using [^{11}C]CH_3I [32, 33].

In Vitro Binding Assays

Blood was taken and spleens were removed from naïve and experimentally *E. multilocularis*-infected animals. Peripheral blood mononuclear cells (PBMCs) were isolated from the blood via Percoll (GE Healthcare Life Science) density gradient centrifugation. The PBMCs were dispersed into 5-ml tubes with a final concentration of 1×10^6/ml in phosphate-buffered saline (DPBS, Life Technologies GmbH, Darmstadt, Germany) supplemented with 1 % bovine serum albumin (BSA, Sigma-Aldrich, St. Louis, MO, USA).

Spleens were washed with PBS and ground through a 70-μm nylon cell strainer in PBS. After washing, the cells were resuspended in 4 ml ACK lysis buffer (Lonza Group AG, Basel, Switzerland) to remove the red blood cells via hypotonic lysis. Splenocytes were then also dispersed into 5-ml tubes with a final concentration of 1×10^6/ml in PBS with 1 % BSA.

An *E. multilocularis* metacestode suspension was prepared by grinding metacestode tissue taken from infected animals through a cell strainer. The cell suspension was washed with PBS and disseminated into 5-ml tubes.

E. multilocularis metacestode vesicles were freshly collected from *in vitro* cell culture and washed three times with PBS, and three vesicles of the same size per sample were dispersed into the 5-ml tubes.

Then, 0.74 MBq of the respective tracer ([^{18}F]FDG, [^{18}F]FLT, [^{18}F]FAZA, and [^{11}C]choline) was added to the cells. The incubation time was 60 min for [^{18}F]FDG and [^{18}F]FAZA, 90 min for [^{18}F]FLT, and 50 min for [^{11}C]choline. The cells were washed three times with PBS supplemented with 1 % BSA, and remaining radioactivity was measured in a Wallac 1480 WIZARD 3″ Gamma Counter (PerkinElmer, Waltham, MA, USA) using an energy window of 350 to 650 keV and was expressed as corrected counts per minute (ccpm).

PET/MR Imaging

E. multilocularis-infected cohorts of gerbils for every tested tracer ($n=5$) were imaged consecutively at an early (2 weeks post-infection (p.i.)) and a late infection time point (6 weeks p.i.). At the early infection time point, only two out of five animals of each cohort showed parasite growth, which led to low animal numbers at this measured time point. Small animal PET scanners (Inveon, Siemens Preclinical Solutions, Knoxville, TN, USA), yielding a spatial resolution of approximately 1.3 mm in the reconstructed images were used for imaging. All animals were shortly anesthetized with isoflurane and injected i.v. with 10–12 MBq of the respective tracer via a lateral tail vein. After tracer injection, static (10 min) or dynamic ([^{18}F]FDG, 65 min; [^{18}F]FLT, 100 min; [^{18}F]FAZA, 70 min; [^{11}C]choline, 70 min) PET scans were. During imaging, for both PET and magnetic resonance (MR) imaging, animals were anesthetized with 1.5 % isoflurane mixed with 100 % oxygen. Depth of anesthesia was monitored by measuring the respiratory rate, and the body temperature was kept at 37 °C using a heating pad. PET data were acquired in list mode, histogrammed in one 10-min time frame, and reconstructed using an iterative ordered subset expectation maximization (OSEM) algorithm without attenuation correction. MR imaging was performed on a 7-T small animal MR tomograph (Clinscan, Bruker Biospin MRI, Ettlingen, Germany) obtaining anatomical information for parasite delineation without using MR contrast agents. A T2-weighted 3D space sequence (TE/TR 202/2,500 ms, image matrix of 137×320, slice thickness 0.27 mm) was used for whole-body imaging. PET images were normalized to each other, subsequently fused to the respective MR images and analyzed using Inveon Research Workplace software (Siemens Preclinical Solutions). Regions of interest (ROIs) were drawn around the parasite and reference (muscle) tissue based on the anatomical information from the MR images. Absolute quantification of the PET data is expressed as percentage of the injected dose (%ID/cc) or as ratios of parasite-to-muscle.

Ex Vivo Biodistribution

Following the final PET scan, the animals were euthanized under deep anesthesia and were subsequently dissected. Parasite tissue and organs were removed and measured together with an aliquot of the injected radiotracer solution by gamma-counting (Wallac 1480 WIZARD 3″ Gamma Counter; PerkinElmer). The results are expressed as percent injected dose per gram of tissue (% ID/g).

Autoradiography and Histology

Metacestode tissue was dissected during the *ex vivo* biodistribution after the final [^{18}F]FDG and [^{18}F]FLT PET scan and was used for digital phosphor storage autoradiography analysis. Metacestode tissue and muscle as reference tissue were frozen at −20 °C in optimal cutting temperature compound (TissueTek O.C.T., Sakura, Zoeterwonde, the Netherlands). Cryosections of 20 µm of the respective tissue samples were exposed to storage phosphor screens (445SI, Molecular Dynamics, Sunnyvale, CA, USA). The readout of the phosphor screens was performed with a STORM Phosphor-Imager (Molecular Dynamics) with a resolution of 50 µm per pixel after an exposure time of 24 h. The same tissue slices used for the autoradiography were stained with hematoxylin and eosin (H&E) following standard procedures [34]. Subsequently, the slides were scanned using the digital slide scanner NanoZoomer 2.0-HT (Hamamatsu Photonics K.K., Hamamatsu, Japan).

Statistical Analysis

Statistical analysis was performed using a two-tailed *t* test. For experiments with more than two investigated groups, statistical significance was calculated using analysis of variance (ANOVA) with post hoc Bonferroni test performed with Origin 8 software (OriginLab Corporation, Northampton, MA, USA). Data were considered statistically significant for $p<0.05$. All quantitative results are shown as the mean±1 standard deviation (SD).

Results

In Vitro Binding Assays

To determine the metabolic potential of *E. multilocularis* metacestode tissue, *in vitro* binding assays were performed with the following tracers: [^{18}F]FDG, [^{18}F]FLT, [^{18}F]FAZA, and [^{11}C]choline. For [^{18}F]FDG consumption of PBMCs and splenocytes of naïve and infected animals, an *E. multilocularis* cell suspension and *E. multilocularis* vesicles were measured after 1 and 3 h of incubation. The overall uptake was significantly elevated with the prolonged incubation time in all samples except for splenocytes from naïve animals and the parasite vesicles (Fig. 1a). The values of those two groups were marginal and therefore negligible. The accumulation of [^{18}F]FDG was highest after the 3-h incubation time for the *E. multilocularis* cell suspension with 303,845±25,651 ccpm followed by splenocytes derived from infected gerbils with 150,650±2,301 ccpm. PBMCs isolated from naïve or infected gerbils displayed similar low glucose uptake values with 33,172±3,645 ccpm (naïve) and 33,895±2,028 ccpm (infected), which were tenfold lower than in the *E. multilocularis* cell suspension (Fig. 1a).

To evaluate the proliferative potential of the parasitic tissue compared to the control cells, samples were incubated with [^{18}F]FLT for 90 min. *E. multilocularis* vesicles presented the highest proliferation rate related to a clearly increased uptake value of 36,078±4,791 ccpm, followed by splenocytes from infected animals with 33,067±2,125 ccpm and the *E. multilocularis* cell suspension with 25,440±2,798 ccpm (Fig. 1b) with higher differences than the control sample PBMCs and splenocytes.

[^{18}F]FAZA accumulation indicates the presence of hypoxic regions within cells and tissue structures. The overall uptake of [^{18}F]FAZA in the above-described experimental setup was consequently low in all tested samples. Only *E. multilocularis* vesicles displayed an elevated uptake of the tracer for hypoxia with 11,364±3,391 ccpm compared to the other tested samples (Fig. 1c).

[^{11}C]choline uptake was higher for *E. multilocularis* vesicles with 50,720±1,333 ccpm reflecting a highly active membrane synthesis compared to PBMC and splenocytes of naïve and infected animals and the *E. multilocularis* cell suspension, which showed only very low [^{11}C]choline accumulation.

PET/MR Imaging

For the *in vivo* evaluation of the respective PET tracers, *E. multilocularis*-infected and naïve animals were injected with [^{18}F]FDG (Fig. 2) or [^{18}F]FLT (Fig. 3) at an early (2 weeks p.i.) and a late (6 weeks p.i.) infection time point. PET quantification showed an increased uptake of [^{18}F]FDG and [^{18}F]FLT 6 weeks after the infection of the animals. The [^{18}F]FDG uptake increased from 0.38±0.20 %ID/cm^3 ($n=2$) at the early infection time point up to 1.03±0.33 %ID/cm^3 ($n=5$; Fig. 2c) at the late infection time point, and [^{18}F]FLT accumulation increased from 0.36±0.22 %ID/cm^3 ($n=2$) to 0.63±0.37 %ID/cm^3 ($n=5$; Fig. 3c). Both groups revealed no significant differences.

The *ex vivo* biodistribution was performed after the last PET/MRI scan for [^{18}F]FDG and [^{18}F]FLT to confirm the quantification obtained from the PET imaging. Parasite tissue and organs were dissected after the final PET scan, and remaining radioactivity was measured in a gamma counter. The data showed an [^{18}F]FDG uptake of 2.62±0.76 %ID/g parasite tissue and an [^{18}F]FLT uptake of 2.50±1.48 (Table 1) %ID/g parasite tissue, which were higher compared to the PET quantification due to partial volume effects and no attenuation correct of the PET images.

PET measurements using [^{18}F]FAZA (Fig. 4a) and [^{11}C]choline (Fig. 4b) were only conducted at the late infection time point in two cohorts of animals ($n=5$), showing no uptake of both tracers in the parasitic lesions. Only background uptake of the tracer [^{18}F]FAZA is observed in the metacestode tissue (data not shown) or no uptake is observed with [^{11}C]choline (data not shown). The tracer [^{11}C]choline revealed higher uptake values than the wrap F-18-labeled tracers due to elevated spillover effects from the liver tissue surrounding the parasite (Fig. 4b).

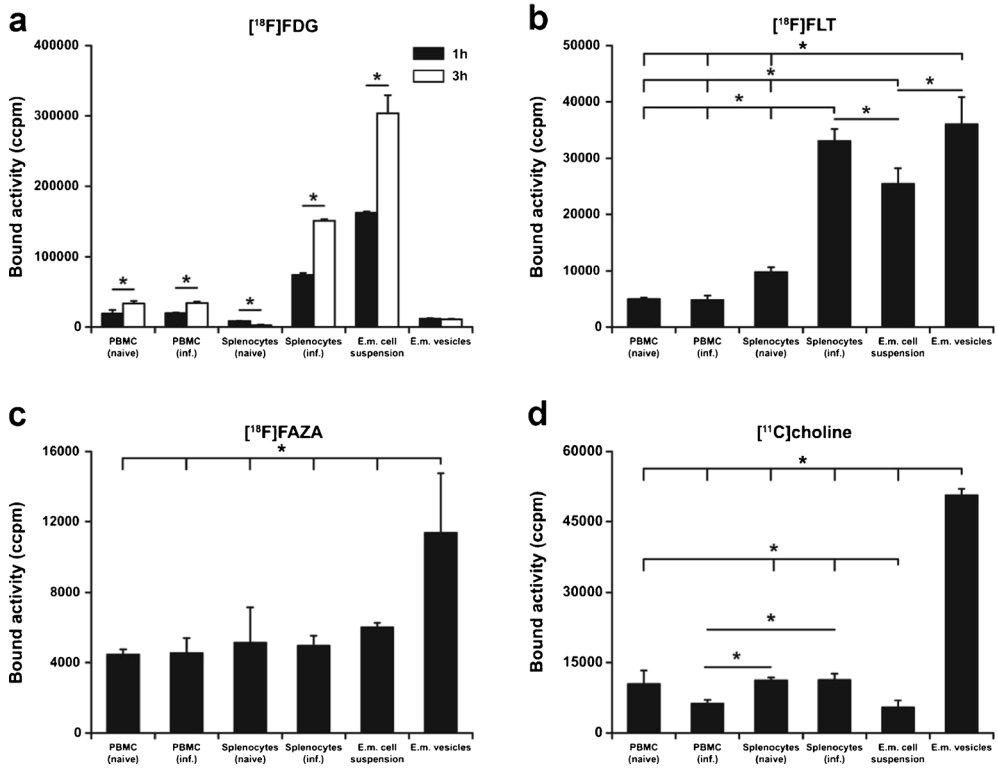

Fig. 1 *In vitro* binding assay of various tracers. **a** *In vitro* binding assays revealed a significantly elevated [^{18}F]FDG uptake in *E. multilocularis* cell suspension and splenocytes of infected animals compared to that of control cells 1 h (*black bars*) and 3 h (*open bars*) after incubation. **b** Assays performed with [^{18}F]FLT showed a significantly increased consumption in *E. multilocularis* cell suspensions and *E. multilocularis* vesicles as well as in splenocytes obtained from infected animals after 90-min incubation. **c** [^{18}F]FAZA accumulation was low in all samples, and only *E. multilocularis* vesicles displayed a significant increased uptake after 1-h incubation. **d** *E. multilocularis* vesicles presented a significantly raised integration of [^{11}C]choline into the cell membranes after 50-min incubation. Data are expressed as ccpm±1 SD and samples are considered statistically significant, with $^{*}p<0.05$.

Autoradiography and Histology

The readout of the autoradiographic analysis showed an increased [^{18}F]FDG (Fig. 5a) and [^{18}F]FLT (Fig. 5e) uptake surrounding the *E. multilocularis* vesicles. H&E staining of the same slices revealed that *E. multilocularis* metacestodes are encircled by infiltrating immune cells indicating inflammation processes and therefore a higher energy consumption (Fig. 5b–d) and proliferative potential (Fig. 5f–h) of the tissue surrounding the metacestode vesicles at the late infection time point.

Discussion

The standard clinical PET tracer [^{18}F]FDG has previously been reported to be useful for the diagnostic and therapy follow-up of AE patients [12, 35]. A more recent advancement especially for the treatment monitoring and diagnosis of active or inactive parasitic lesions is delayed [^{18}F]FDG-PET. Although delayed [^{18}F]FDG-PET is still not a gold standard tool, it achieved sufficient results in the discrimination of viable parasite tissue compared to dead tissue when combined with serological tests [18]. This decision becomes important when selecting patients where chemotherapeutic treatment with BZM is parasitocidal and a discontinuation of treatment is taken into account. Early disruption of treatment may cause recurrence of the metabolic activity and further growth of *E. multilocularis* lesions. Therefore, it is necessary for clinicians to determine the appropriate time point of ending the therapy to reduce the serious side effects and the psychological burden of lifelong treatment and to decrease the extensive costs for the healthcare sector [13, 35]. Nevertheless, small lesions are consistently detected with less reliability, especially in organs with high background activity such as the liver, which possibly leads to false-negative findings. Another scenario involves patients with impaired immunity being seronegative for *E. multilocularis*-specific ELISAs but still carrying viable parasitic tissue [13].

Our preclinical investigations showed, as others have seen in clinical settings [12, 13, 18], that the increased [^{18}F]FDG uptake, represented as focal tracer accumulation (“hot spots”), is caused by an inflammatory immune reaction located around the parasitic lesions. Based on the autoradiography and histology results, we were able to show that the [^{18}F]FDG uptake we observed in late stage infected animals was due to several foci of inflammation rather than specific

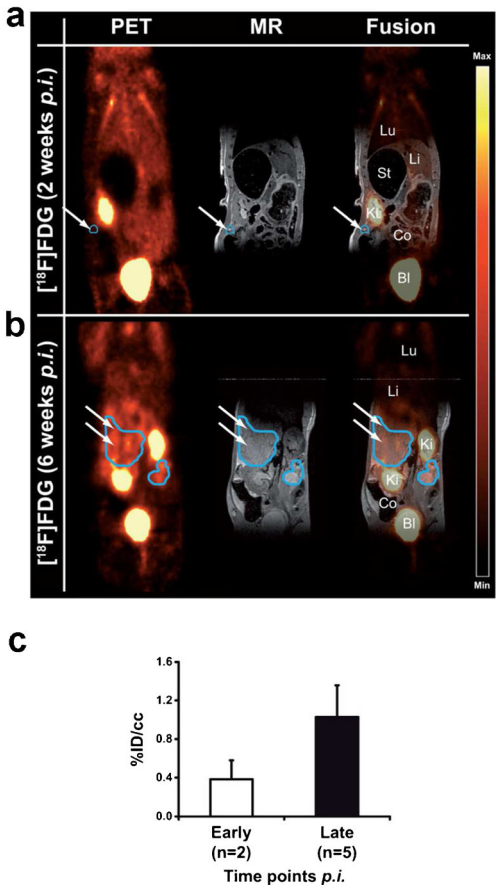

Fig. 2 Coronal [^{18}F]FDG-PET, MR, and fused images from early (2 weeks p.i., **a**) and late (6 weeks p.i., **b**) stage *E. multilocularis* metacestode-infected gerbils. *Arrows* and *blue lines* indicate the positions of the metacestode tissue (*Bl*: bladder; *Co*: colon; *Ki*: kidney; *Li*: liver; *Lu*: lung; *Sp*: spleen; *St*: stomach). **c** Quantification of the PET images revealed an increase in tracer accumulation at the late infection stage in areas of the parasite tissue. Lower uptake of [^{18}F]FDG is observed in metacestodes in the early infection stage. The results are shown as %ID/cc and *error bars* represent SD.

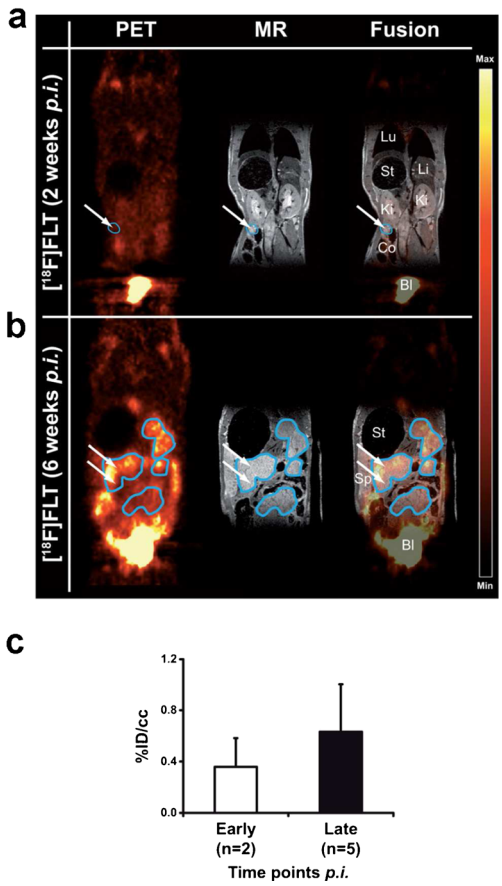

Fig. 3 Coronal [^{18}F]FLT PET, MR, and fused images from early (2 weeks p.i., **a**) and late (6 weeks p.i., **b**) stage *E. multilocularis* metacestode-infected gerbils. *Arrows* and *blue lines* indicate the positions of the metacestode tissue (*Bl*: bladder; *Co*: colon; *Ki*: kidney; *Li*: liver; *Lu*: lung; *Sp*_ spleen; *St*: stomach). **c** Quantification of the PET images revealed an increase in tracer accumulation at the late infection stage in areas of the parasite tissue. Lower uptake of [^{18}F]FLT is observed in metacestodes in the early infection stage. The results are shown as %ID/cc and *error bars* represent SD.

uptake in the parasite tissue. In particular, the histological examination revealed infiltrating immune cells around the vesicles forming the periparasitic region. In immunosuppressed patients, this periparasitic region is characterized by a decreased number of immune cells leading to false-negative PET-CT diagnosis [13]. Hence, it seems likely that very small lesions or lesions with low metabolic activity are not detected reliably which, in the worst case, could lead to further disease progression after therapy interruption. The clinical standard PET tracer [^{18}F]FDG for imaging malignancies plays an important role for imaging infectious diseases or their inflammation processes [36]. Again, a specific diagnosis of the disease with [^{18}F]FDG is not possible, and mainly the accumulation of glucose-consuming immune cells with enhanced metabolic activity in the inflamed tissue can be localized [37]. Particularly in the field of preclinical imaging, an increasing number of

Table 1. *Ex vivo* biodistribution of organs of *E. multilocularis*-infected gerbils (n=5). The animals were injected with 10–12 MBq [^{18}F]FDG or [^{18}F]FLT at the late stage of the infection. Tissues were excised and measured 1 h ([^{18}F]FDG) or 90 min ([^{18}F]FLT) after the injection. Data are %ID/g, expressed as the mean or as parasite-to-liver or parasite-to-muscle ratios±1 SD

%ID/g		
	[^{18}F]FDG	[^{18}F]FLT
Blood	0.42±0.06	0.60±0.58
Heart	22.70±2.29	0.53±0.47
Parasite	2.62±0.76	2.50±1.48
Spleen	3.43±0.93	2.73±3.04
Liver	0.81±0.08	0.74±0.63
Stomach	1.06±0.32	0.54±0.31
Colon	1.60±0.26	1.18±0.64
Kidney	4.06±1.59	1.78±1.49
Brain	3.16±0.34	0.36±0.39
Muscle	0.61±0.33	0.62±0.46
Parasite/muscle	4.31±2.27	4.07±3.25

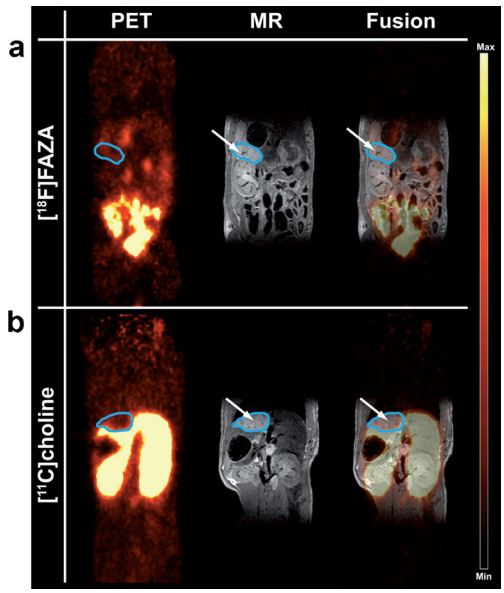

Fig. 4 **a** Coronal [^{18}F]FAZA and **b** [^{11}C]choline PET, MR, and fused images from late (6 weeks p.i.) stage *E. multilocularis* metacestode-infected gerbils. *Arrows* and *blue lines* indicate the positions of the metacestode tissue. Only background uptake of these tracers is observed in the parasite tissue.

biomarkers, including monoclonal antibodies or their fragments, peptides, and small molecules are developed and tested for imaging infectious diseases. Compared to cancer research, the tracer development for detecting pathogens such as viruses, bacteria, fungi, and parasites is still a niche [38, 39].

The aim of the study was to evaluate various PET tracers for the detection and diagnosis of AE in an animal model. The elevated uptake of [^{18}F]FLT we observed *in vitro* in splenocytes of infected animals and in the *E. multilocularis* cell suspension can be traced back to the proliferative potential of activated immune cells from the periparasitic region. This was proven by the autoradiographic images, where the uptake correlated well with immune cells accumulating around the parasite vesicles observed in histological investigations of the same tissue slices. Pure *E. multilocularis* vesicles showed the highest uptake for [^{18}F]FLT, which can be explained by the natural proliferative activity of the vesicles itself. As reported by Koziol *et al.*, only germinative cells proliferate in the larval vesicles [40]. With the utmost probability, those cells are responsible for the [^{18}F]FLT uptake. Our *in vivo* findings with [^{18}F]FLT in late stage infected gerbils resembled the uptake pattern we observed in the [^{18}F]FDG studies with elevated uptake values represented as focal enhancement throughout the parasitic mass. Those "hot spots" are caused by inflammatory processes, as evidenced by the proliferation of activated immune cells, within the periparasitic area of the lesions; the observed uptake of [^{18}F]FDG and [^{18}F]FLT corresponds to the unspecific accumulation of the respective tracer in the inflamed regions of the parasite tissue.

In preclinical settings and in patients, [^{18}F]FAZA is a widely studied PET tracer for the identification of hypoxic areas within tumors [31, 41, 42]. Although there have been reports of hypoxia playing an important role in infectious diseases, [^{18}F]FAZA has not been used to date for the

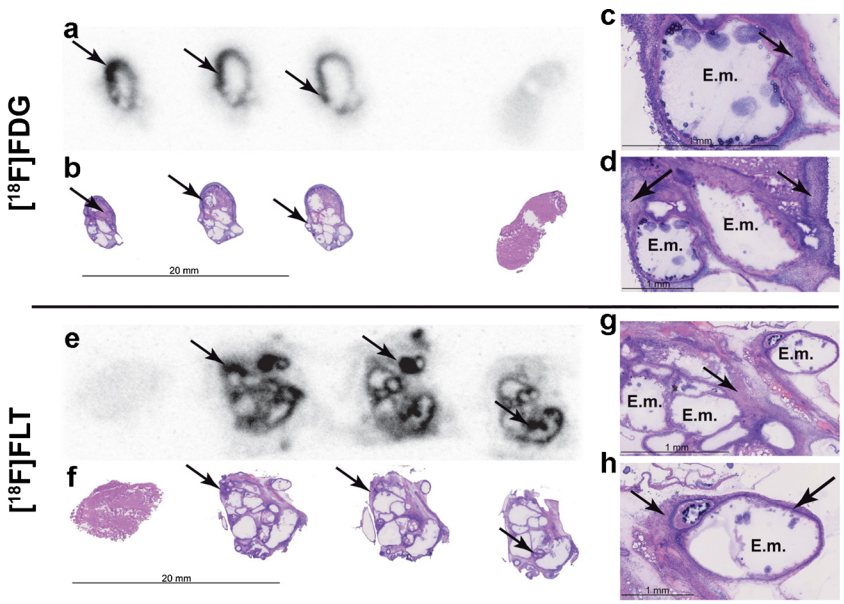

Fig. 5 Autoradiography of 20-µm *E. multilocularis* metacestode and muscle tissue sections obtained after the last **a** [^{18}F]FDG and **e** [^{18}F]FLT PET scans and at the late infection stage (6 weeks p.i.). For both tracers, accumulation is observed in the surrounding tissue of the parasite but not in the metacestode itself. Representative H&E staining of the same slices used for autoradiography depicts inflammatory processes in the form of accumulation of immune cells next to the metacestode (*E.m.*) and are reason for the tracer accumulation in the inflamed parasite tissue [^{18}F]FDG: **b**–**d**; [^{18}F]FLT: **f**–**h**). *Arrows* indicate the infiltrated inflammatory cells.

detection of infected areas. Our *in vitro* binding assays displayed a slightly elevated uptake of [^{18}F]FAZA in *E. multilocularis* vesicles. Based on the *in vivo* studies with *E. multilocularis*-infected gerbils, this tracer is not applicable for the detection of *E. multilocularis* parasitic lesions.

Jian et al. performed proton magnetic resonance spectroscopy (^{1}HMRS) on parasitic brain lesions in patients with cerebral alveolar echinococcosis (CAE) [43]. Concentrations of various metabolites in CAE lesions were investigated, and their changes depending on the region of the parasitic mass were recorded. Choline was found to have the highest concentration in the substantial area of the lesions.

Furthermore, Wyass et al. reported on the high accumulation of [^{18}F]choline in inflammatory infiltrates caused by the bacterium *Staphylococcus aureus* [44]. Marangoni et al. confirmed those findings and investigated the usefulness of [^{11}C]choline as a PET tracer in genital chlamydial infections in mice and verified the pathogen-specific proliferation mechanisms of proliferating inflammatory cells [45]. We discovered a high uptake of [^{11}C]choline in *E. multilocularis* vesicles in our *in vitro* binding assays because choline is quickly integrated as a precursor for the biosynthesis of phospholipids, which are important components of all membranes [23]. However, our *in vivo* studies with [^{11}C]choline showed no accumulation in the parasitic lesions in late stage AE-infected animals.

A drawback is that [^{11}C]choline is massively taken up by the liver cells, and it turned out to be not suitable for the detection of small parasitic lesions, which usually have their origin within the liver. The preclinical findings of this study lead to our assumption that it seems impossible to detect small hepatic lesions in AE patients with the [^{11}C]choline PET tracer.

Conclusion

In conclusion, our study demonstrates the variety of clinically used PET tracers [^{18}F]FDG, [^{18}F]FLT, [^{18}F]FAZA, and [^{11}C]choline) in AE infection in gerbils. Whereas our *in vitro* binding assays displayed great potential of the various tracers to supplement current diagnostic and therapy monitoring strategies, the *in vivo* investigations confirmed that AE lesions are still difficult to discover, and the determination between viable and non-active parasitic tissue remains a challenge. All tested tracers are only specific to inflammatory processes at the site of infection but not to the pathogen itself. Therefore, further research is needed to develop new pathogen-specific diagnostic tools to ameliorate therapeutic decisions, to improve the quality of life for the patients, and to reduce costs for the healthcare sector.

Acknowledgments. This research was supported by the Deutsche Forschungsgemeinschaft (grant WI 3777/1-1), and PTS and WHH were supported by the European Commission FP7 Grant EPIAF #242131. We are grateful to Denis Lamparter, Walter Ehrlichmann, and Anke Stahlschmidt for producing the PET tracers. We thank Maren Harant for expert technical assistance.

Conflict of Interest. Bernd J. Pichler: grant/research support: Siemens, AstraZeneca, Bayer Healthcare, Boehringer-Ingelheim, Oncodesign, Merck, Bruker. Other authors: no conflicts of interest.

References

1. Eckert J, Deplazes P (2004) Biological, epidemiological, and clinical aspects of echinococcosis, a zoonosis of increasing concern. Clin Microbiol Rev 17:107–135
2. Tappe D, Kern P, Frosch M (2010) A hundred years of controversy about the taxonomic status of Echinococcus species. Acta Trop 115:167–174
3. Knapp J, Bart JM, Giraudoux P et al (2009) Genetic diversity of the cestode Echinococcus multilocularis in red foxes at a continental scale in Europe. PLoS Negl Trop Dis 3:e452
4. Gover L, Kirkbride H, Morgan D (2011) Public health argument to retain current UK national controls for tick and tapeworms under the Pet Travel Scheme. Zoonoses Public Health 58:32–35
5. Brunetti E, Kern P, Vuitton DA (2010) Expert consensus for the diagnosis and treatment of cystic and alveolar echinococcosis in humans. Acta Trop 114:1–16
6. Tuzun M, Altinors N, Arda IS, Hekimoglu B (2002) Cerebral hydatid disease CT and MR findings. Clin Imaging 26:353–357
7. Mejri N, Hemphill A, Gottstein B (2010) Triggering and modulation of the host-parasite interplay by Echinococcus multilocularis: a review. Parasitology 137:557–568
8. Vuitton DA, Gottstein B (2010) Echinococcus multilocularis and its intermediate host: a model of parasite-host interplay. J Biomed Biotechnol 2010:923193
9. (1996) Guidelines for treatment of cystic and alveolar echinococcosis in humans. WHO Informal Working Group on Echinococcosis. Bull World Health Organ 74:231–242
10. Kern P (2010) Clinical features and treatment of alveolar echinococcosis. Curr Opin Infect Dis 23:505–512
11. Stettler M, Rossignol JF, Fink R et al (2004) Secondary and primary murine alveolar echinococcosis: combined albendazole/nitazoxanide chemotherapy exhibits profound anti-parasitic activity. Int J Parasitol 34:615–624
12. Reuter S, Schirrmeister H, Kratzer W et al (1999) Pericystic metabolic activity in alveolar echinococcosis: assessment and follow-up by positron emission tomography. Clin Infect Dis 29:1157–1163
13. Azizi A, Blagosklonov O, Lounis A et al (2014) Alveolar echinococcosis: correlation between hepatic MRI findings and FDG-PET/CT metabolic activity. Abdom Imaging
14. Czermak BV, Akhan O, Hiemetzberger R et al (2008) Echinococcosis of the liver. Abdom Imaging 33:133–143
15. Reuter S, Buck A, Manfras B et al (2004) Structured treatment interruption in patients with alveolar echinococcosis. Hepatology 39:509–517
16. Stumpe KD, Renner-Schneiter EC, Kuenzle AK et al (2007) F-18-Fluorodeoxyglucose (FDG) positron-emission tomography of Echinococcus multilocularis liver lesions: prospective evaluation of its value for diagnosis and follow-up during benzimidazole therapy. Infection 35:11–18
17. Ehrhardt AR, Reuter S, Buck AK et al (2007) Assessment of disease activity in alveolar echinococcosis: a comparison of contrast enhanced ultrasound, three-phase helical CT and [(18)F] fluorodeoxyglucose positron emission tomography. Abdom Imaging 32:730–736
18. Caoduro C, Porot C, Vuitton DA et al (2013) The role of delayed ^{18}F-FDG PET imaging in the follow-up of patients with alveolar echinococcosis. J Nucl Med 54:358–363
19. Kumar R, Basu S, Torigian D et al (2008) Role of modern imaging techniques for diagnosis of infection in the era of ^{18}F-fluorodeoxyglucose positron emission tomography. Clin Microbiol Rev 21:209–224
20. Macheda ML, Rogers S, Best JD (2005) Molecular and cellular regulation of glucose transporter (GLUT) proteins in cancer. J Cell Physiol 202:654–662
21. Rodriguez-Enriquez S, Marin-Hernandez A, Gallardo-Perez JC, Moreno-Sanchez R (2009) Kinetics of transport and phosphorylation of glucose in cancer cells. J Cell Physiol 221:552–559
22. Shields AF, Grierson JR, Dohmen BM et al (1998) Imaging proliferation in vivo with [F-18]FLT and positron emission tomography. Nat Med 4:1334–1336

23. Hara T (2002) 11C-choline and 2-deoxy-2-[^{18}F]fluoro-D-glucose in tumor imaging with positron emission tomography. Mol Imaging Biol 4:267–273
24. Marik J, Junutula JR (2011) Emerging role of immunoPET in receptor targeted cancer therapy. Curr Drug Deliv 8:70–78
25. Kuster T, Hermann C, Hemphill A et al (2013) Subcutaneous infection model facilitates treatment assessment of secondary alveolar echinococcosis in mice. PLoS Negl Trop Dis 7:e2235
26. Eger A, Kirch A, Manfras B et al (2003) Pro-inflammatory (IL-1beta, IL-18) cytokines and IL-8 chemokine release by PBMC in response to Echinococcus multilocularis metacestode vesicles. Parasite Immunol 25:103–105
27. Hubner C, Wiehr S, Kocherscheidt L et al (2010) Effects of in vitro exposure of Echinococcus multilocularis metacestodes to cytostatic drugs on in vivo growth and proliferation of the parasite. Parasitol Res 107:459–463
28. Judenhofer MS, Wehrl HF, Newport DF et al (2008) Simultaneous PET-MRI: a new approach for functional and morphological imaging. Nat Med 14:459–465
29. Reischl G, Blocher A, Wei R et al (2006) Simplified, automated synthesis of 3′-[^{18}F]fluoro-3′-deoxy-thymidine ([^{18}F]FLT) and simple method for metabolite analysis in plasma. Radiochim Acta 94:447–451
30. Hamacher K, Coenen HH, Stocklin G (1986) Efficient stereospecific synthesis of no-carrier-added 2-[^{18}F]-fluoro-2-deoxy-D-glucose using aminopolyether supported nucleophilic substitution. J Nucl Med 27:235–238
31. Maier FC, Kneilling M, Reischl G et al (2011) Significant impact of different oxygen breathing conditions on noninvasive in vivo tumor-hypoxia imaging using [(1)(8)F]-fluoro-azomycinarabino-furanoside ([(18)F]FAZA). Radiat Oncol 6:165
32. Reischl G, Bieg C, Schmiedl O, Solbach C, Machulla HJ (2004) Highly efficient automated synthesis of [(11)C]choline for multi dose utilization. Appl Radiat Isot 60:835–838
33. Kukuk D, Reischl G, Raguin O et al (2011) Assessment of PET tracer uptake in hormone-independent and hormone-dependent xenograft prostate cancer mouse models. J Nucl Med 52:1654–1663
34. Kneilling M, Hultner L, Pichler BJ et al (2007) Targeted mast cell silencing protects against joint destruction and angiogenesis in experimental arthritis in mice. Arthritis Rheum 56:1806–1816
35. Reuter S, Gruner B, Buck AK et al (2008) Long-term follow-up of metabolic activity in human alveolar echinococcosis using FDG-PET. Nuklearmedizin 47:147–152
36. Jamar F, Buscombe J, Chiti A et al (2013) EANM/SNMMI guideline for ^{18}F-FDG use in inflammation and infection. J Nucl Med 54:647–658
37. del Rosal T, Goycochea WA, Mendez-Echevarria A et al (2013) (18)F-FDG PET/CT in the diagnosis of occult bacterial infections in children. Eur J Pediatr 172:1111–1115
38. Glaudemans AW, Quintero AM, Signore A (2012) PET/MRI in infectious and inflammatory diseases: will it be a useful improvement? Eur J Nucl Med Mol Imaging 39:745–749
39. Wehrl HF, Wiehr S, Divine MR et al (2014) Preclinical and translational PET/MR imaging. J Nucl Med 55:11S–18S
40. Koziol U, Rauschendorfer T, Zanon Rodriguez L et al (2014) The unique stem cell system of the immortal larva of the human parasite Echinococcus multilocularis. Evodevo 5:10
41. Sorger D, Patt M, Kumar P et al (2003) [^{18}F]Fluoroazomycinarabino-furanoside (18FAZA) and [^{18}F]fluoromisonidazole (18FMISO): a comparative study of their selective uptake in hypoxic cells and PET imaging in experimental rat tumors. Nucl Med Biol 30:317–326
42. Beck R, Roper B, Carlsen JM et al (2007) Pretreatment ^{18}F-FAZA PET predicts success of hypoxia-directed radiochemotherapy using tirapazamine. J Nucl Med 48:973–980
43. Wang J, Yao WH, Yi BN et al (2012) Proton magnetic resonance spectroscopy in the evaluation of infiltration zone of cerebral alveolar echinococcosis. Chin Med J (Engl) 125:2260–2264
44. Wyss MT, Weber B, Honer M et al (2004) ^{18}F-choline in experimental soft tissue infection assessed with autoradiography and high-resolution PET. Eur J Nucl Med Mol Imaging 31:312–316
45. Marangoni A, Nanni C, Quarta C et al (2013) Usefulness of ^{11}C-choline positron emission tomography for genital chlamydial infection assessment in a BALB/c murine model. Mol Imaging Biol 15:450–455